Available online at www.sciencedirect.com
SCIENCE DIRECT®
International Journal of Heat and Mass Transfer 47 (2004) 3957–3969
International Journal of HEAT and MASS TRANSFER
www.elsevier.com/locate/ijhmt

Hydrodynamic and thermal oscillations in a non-isothermal laminar jet

S. Suyambazhahan, Sarit K. Das *, T. Sundararajan

Heat Transfer and Thermal Power Laboratory, Department of Mechanical Engineering, Indian Institute of Technology Madras, Chennai 600 036, India

Received 31 December 2002; received in revised form 26 December 2003

Abstract

Oscillations in two-dimensional laminar jets have been studied numerically over a wide range of Reynolds and Grashof numbers. A finite volume approach based on primitive variables has been adopted. The numerical scheme is first validated using available experimental data for both the mean flow and the oscillatory behavior of isothermal jets, and then it is used to simulate results of the present study. The results indicate a strong spatial dependence of amplitude and existence of a broad band of frequencies, particularly in non-isothermal jets. High frequency oscillations are observed for forced convection dominated situations, while low frequency oscillations occur when buoyancy effects are predominant. With increasing buoyancy effect, the amplitudes are significantly modified and the oscillations become non-periodic even at low Reynolds number. The jet orientation is also found to influence the spectral distribution of oscillations. The predicted results can be significant in practical applications to devices in which mixing of non-isothermal jets occurs.
© 2004 Elsevier Ltd. All rights reserved.

1. Introduction

Jet flows are encountered in a variety of industrial applications and physical situations. Aerospace vehicles employ jets for the generation of thrust and for other purposes such as thrust vectoring, noise control etc. In combustion appliances, fuel and oxidizer are be mixed in the form of jets for achieving efficient combustion. Jets are also employed in various manufacturing and metallurgical processes, impingement cooling of electronic devices and in fluidic devices such as ejectors. In many of these applications, the flow field may be non-isothermal and may experience both forced and free convective effects. Also, oscillations could occur in the velocity and temperature fields due to convective instabilities arising in the jet shear layers. As a consequence, in systems such as nuclear reactor core, cyclically varying thermal stresses are often observed in regions where jets of different temperatures mix. Thus, the flow and temperature oscillations may eventually lead to structural failure, known as thermal striping [1].

Experimental studies on the oscillatory flow behavior of free and confined two-dimensional jets have been carried out by several authors [2–5]. Theoretical analyses of axi-symmetric flow development in free jets have been performed by Batchelor and Gill [6] and Cohen and Wygnanski [7]. Recently, Sarma et al. [8] presented a numerical simulation of laminar confined jet flows. They delineated the ranges of Reynolds number and aspect ratio values for which the confined jet may spread asymmetrically as an attached wall jet or as temporally oscillating flow. Instabilities associated with non-circular jets have been described by several authors [9–13]. A few studies are also available on the spreading features of non-isothermal jets [14,15]. A majority of the works described above deal with experimental measurements and available detailed theoretical studies on jet spreading characteristics are very few. Also, the effect of

* Corresponding author. Tel.: +91-44-2257-8550.
E-mail addresses: sarit_das@hotmail.com, skdas@iitm.ac.in (S.K. Das).

0017-9310/$ - see front matter © 2004 Elsevier Ltd. All rights reserved.
doi:10.1016/j.ijheatmasstransfer.2004.01.010

Nomenclature

c_p	specific heat capacity [J kg^{-1} K^{-1}]
d_j	jet width [m]
f	frequency [Hz]
g	acceleration due to gravity [m s^{-2}]
Gr	Grashof number $[g\beta(T_j - T_0)d_j^3/v^2]$
k	thermal conductivity [w m^{-1} K]
n_x, n_y	components of surface normal
p	pressure [N m^{-2}]
Re	Reynolds number $[u_j d_j/v]$
Ri	Richardson number $[Gr/Re^2]$
S	Strouhal number $[fd_j/u_j]$
t	time [s]
t^*	non-dimensional time $[tu_j/d_j]$
T_j	jet inlet temperature [K]
T	temperature [K]
u, v	velocity components [m s^{-1}]
u_j	jet inlet velocity [m s^{-1}]
u/u_j	non-dimensional x velocity
x, y	space co-ordinates [m]
y_j	jet height [m]
$y_{0.5}$	local jet half width [m]

Greek symbols

β	thermal expansion coefficient [K^{-1}]
v	kinematic viscosity [m^2 s^{-1}]
θ	non-dimensional temperature $[T - T_0]/[T_j - T_0]$
ρ	density of air [kg m^{-3}]
σ	stress [N m^{-2}]

Subscripts

0	ambient
x, y	for x or y direction component

combined forced and free convective flow on the velocity and temperature oscillations of a non-isothermal jet have not been studied so far. In the present study, a numerical simulation of non-isothermal oscillations of laminar, incompressible planar jets are considered. The effects of both forced and natural convective phenomena are highlighted, for upward, downward and horizontal jet flow configurations.

2. Numerical model

A planar gas jet issuing from a nozzle with a fully developed laminar velocity profile into a stationary medium of infinite extent is considered. The inlet Reynolds number of the jet is of the order of 100. Since the jet Reynolds number based on local velocity and jet width (as seen from the numerical results presented later) also remains of the order of 100, it is assumed that the jet is laminar over the whole computational domain. The jet fluid is taken to be hotter than the ambient medium ($T_j > T_0$), and both fluids are assumed to be air. For simulation purposes, the computational domain is truncated at a distance of about 10 diameters from the mid-plane in the lateral direction and at a distance ranging between 100 and 300 jet widths in the axial direction (Fig. 1). In order to capture the unsteady oscillations of the jet, symmetry about the mid-plane is not assumed and a full domain including regions on either side of the plane is considered. The density variation in the non-isothermal flow field is modeled according to the Boussinesq approximation and the direction of gravity with respect to the flow direction is prescribed depending on the flow configuration i.e. up-

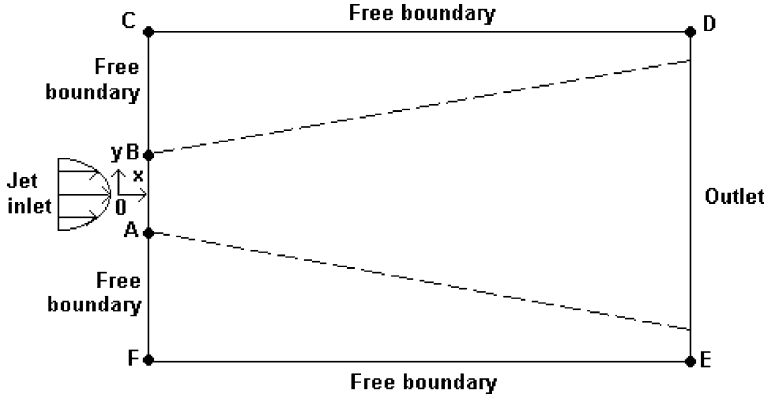

Fig. 1. Geometry of the problem.

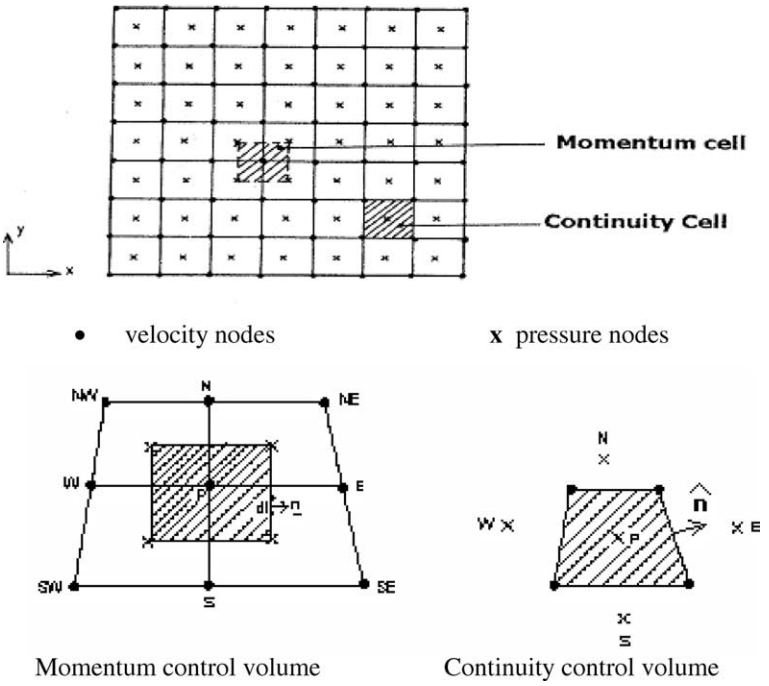

Fig. 2. Staggered grid structure.

ward, downward or horizontal jet. The governing equations for the unsteady flow and heat transfer in integral form for each computational cell (Fig. 2) can be written as

Continuity equation

$$\oint (\underline{v}\cdot\underline{n})\,\mathrm{d}l = \oint (un_x + vn_y)\,\mathrm{d}l = 0 \tag{1}$$

where n_x and n_y are the directional cosines of the local normal on the boundary and (u, v) are the velocity components in x and y directions.

x-momentum equation

$$\oint\oint \rho_0 \frac{\partial u}{\partial t}\,\mathrm{d}x\,\mathrm{d}y + \oint \rho_0 u(un_x + vn_y)\,\mathrm{d}l = \oint (\sigma_{xx}n_x + \sigma_{xy}n_y)\,\mathrm{d}l + \int\int \rho g_x\,\mathrm{d}x\,\mathrm{d}y \tag{2}$$

y-momentum equation

$$\int\int \rho_0 \frac{\partial v}{\partial t}\,\mathrm{d}x\,\mathrm{d}y + \oint \rho_0 v(un_x + vn_y)\,\mathrm{d}l = \oint (\sigma_{yx}n_x + \sigma_{yy}n_y)\,\mathrm{d}l + \int\int \rho g_y\,\mathrm{d}x\,\mathrm{d}y \tag{3}$$

Here, ρ_0 and ρ are the average and local density values, and g_x, g_y are the components of the gravitational acceleration vector $\underline{g}$. Also, the stresses are given by

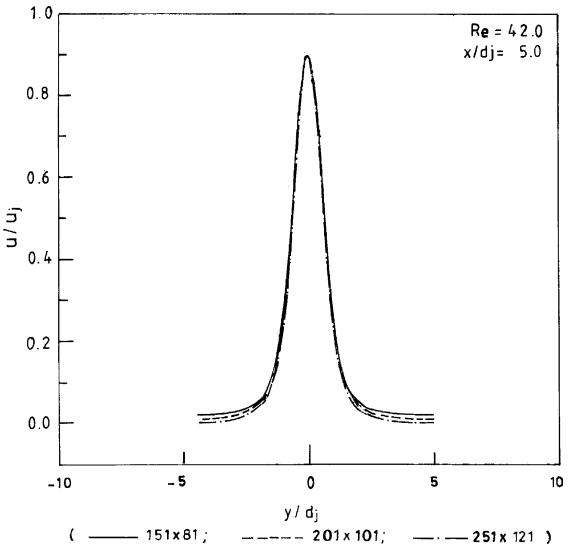

Fig. 3. Grid independence study.

$$\sigma_{xx} = -p + 2\mu\frac{\partial u}{\partial x}, \quad \sigma_{yy} = -p + 2\mu\frac{\partial v}{\partial y}$$

and

$$\sigma_{xy} = \sigma_{yx} = \mu\left(\frac{\partial u}{\partial y} + \frac{\partial v}{\partial x}\right).$$

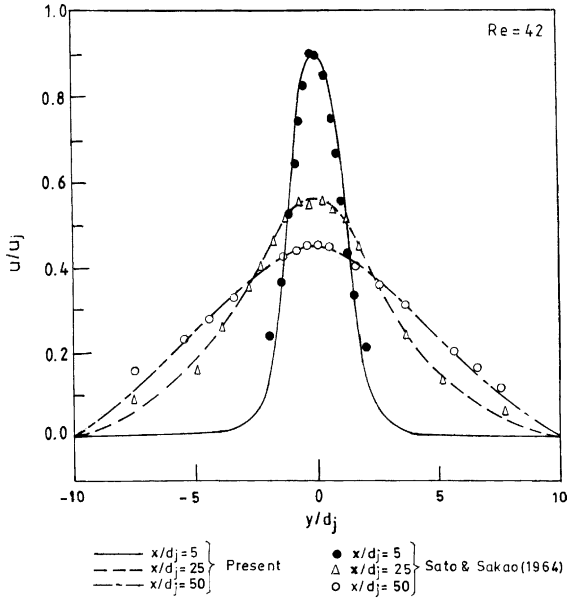

Fig. 4. Validation of numerical predictions with experimental data for mean velocity profiles.

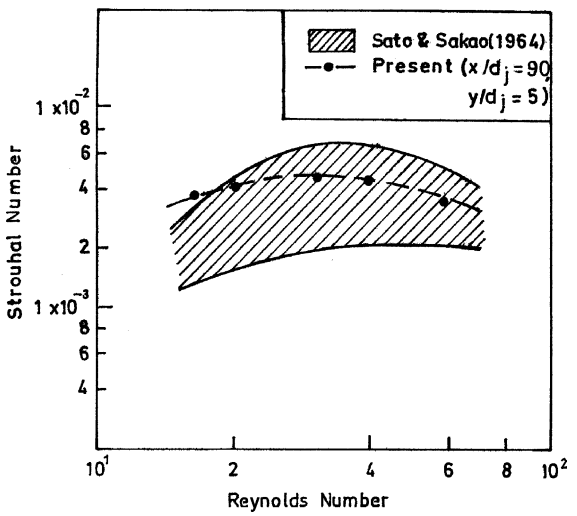

Fig. 5. Validation of Strouhal number predictions for isothermal jet flow.

Heat balance equation

$$\rho_0 c_p \left[\int\int \frac{\partial T}{\partial t} \,\mathrm{d}x\,\mathrm{d}y + \oint T(un_x + vn_y)\,\mathrm{d}l \right] = k \oint \left(\frac{\partial T}{\partial x} n_x + \frac{\partial T}{\partial y} n_y \right) \mathrm{d}l \tag{4}$$

In the above equations, all fluid properties are assumed to be constant except for density in the body force term. Density is determined in terms of the local temperature using the relation

$$\rho_0 - \rho = \rho_0 \beta (T - T_0) \tag{5}$$

The boundary conditions prescribed for the simulation of jet flow are shown in Fig. 1. At the nozzle exit (AB), a fully developed laminar (parabolic) velocity profile is prescribed in the form

$$u = u_0 \left(1 - \frac{y^2}{y_j^2} \right) \quad \text{and} \quad v = 0, \ \text{where } y_j = 0.5 d_j \tag{6a}$$

The jet fluid temperature at entry is taken as uniform and equal to T_j. On the free boundaries (BC, CD, AF and FE), the total pressure is prescribed as

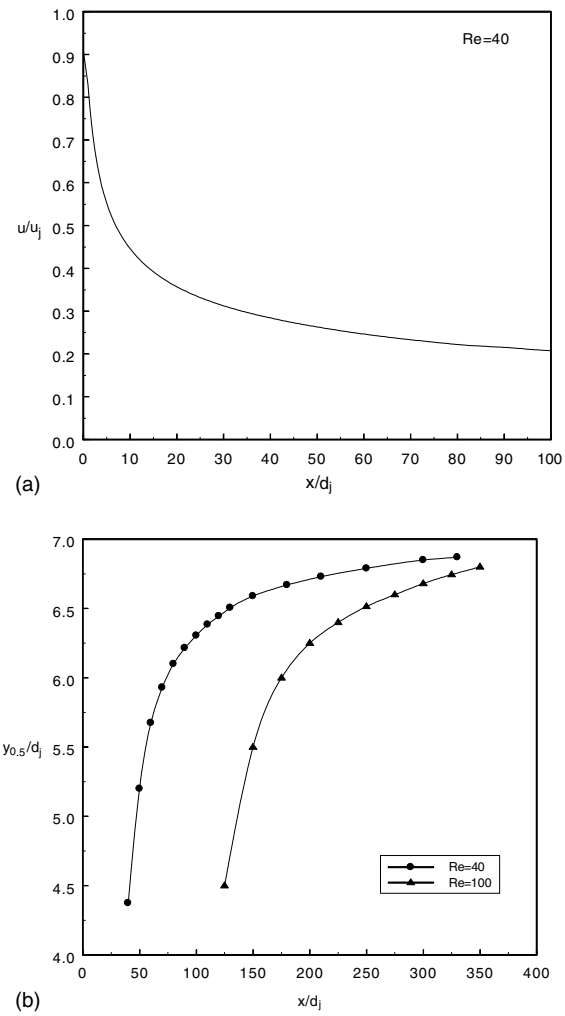

Fig. 6. (a) Axial centerline velocity distribution along the jet and (b) axial variation of jet half width.

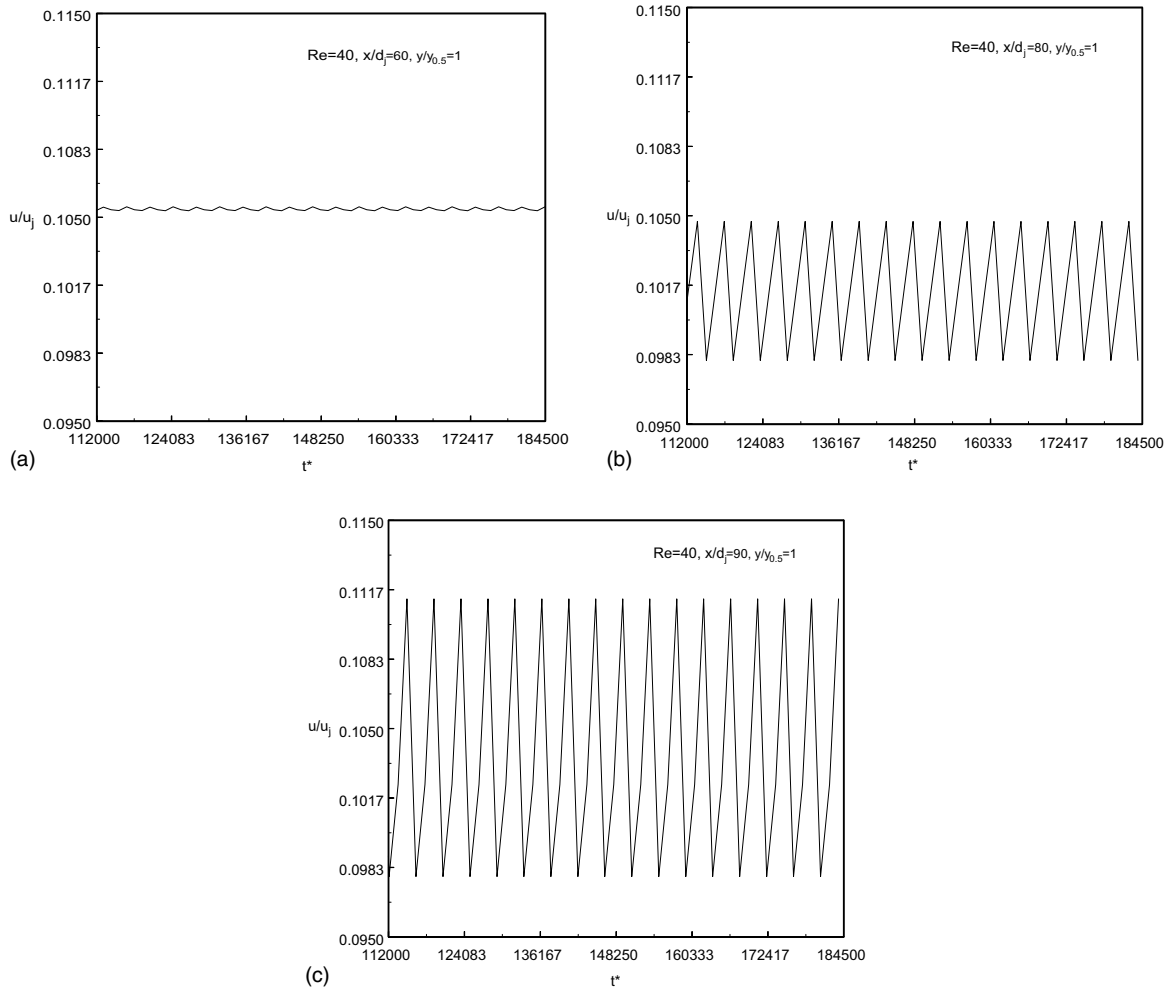

Fig. 7. Axial velocity oscillations: (a) $[x/d_j = 60]$, (b) $[x/d_j = 80]$ and (c) $[x/d_j = 90]$.

$$p + \tfrac{1}{2}\rho_0(u^2 + v^2) = p_0 \tag{6b}$$

where p_0 is the ambient pressure, if the flow enters into the domain. Also, the fluid temperature is prescribed as the ambient value T_0. The other variables are extrapolated from the interior solution. If flow leaves the computational domain at the free boundary, all solution variables are extrapolated from the interior, with some smoothening applied between the values at neighbouring boundary nodes. At the exit boundary (DE), the second derivative of each variable (ϕ) in the flow direction has been set as zero. Hence

$$\frac{\partial^2\phi}{\partial x^2} = 0 \tag{6c}$$

where ϕ may be u, v or T. In fact, the prescription of a convective boundary condition in the form

$$\frac{\partial\phi}{\partial t} + u\frac{\partial\phi}{\partial x} = 0 \tag{6d}$$

gives an almost identical solution as that in the case of boundary condition (6c).

A semi-implicit finite volume scheme based on the SIMPLE technique [16] has been employed to solve the above system of equations. As the details of the numerical scheme have been described elaborately elsewhere [17], only the salient features of the method are summarized here for the sake of brevity. In the integral form of governing equations, the convective and diffusion terms are approximated at cell boundaries, while the source and storage terms are evaluated through a lumped approximation at the cell centre. The momentum equations are solved by time marching, treating the pressure alone implicitly and the other terms explicitly. The pressure is updated via the continuity equation, by

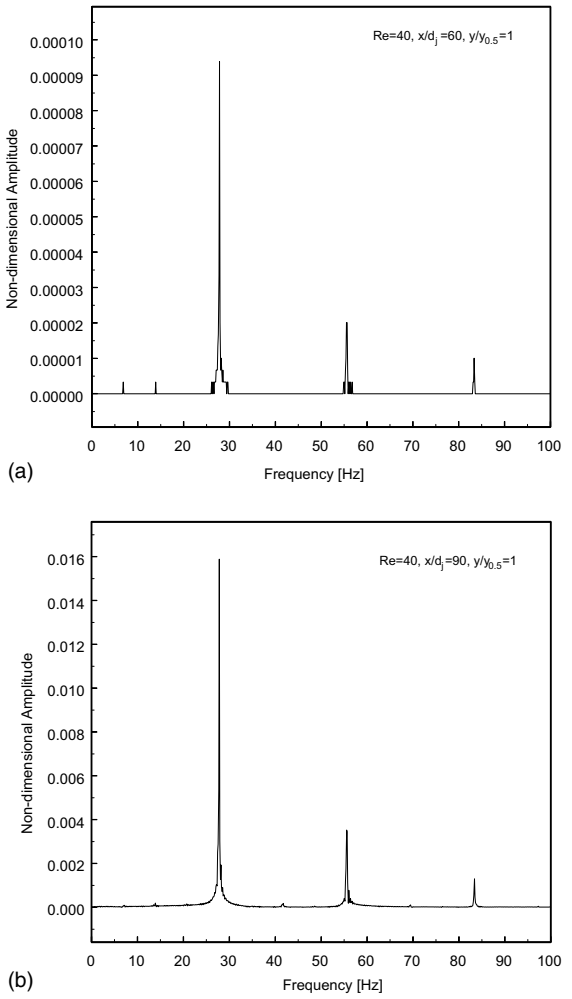

Fig. 8. FFT analysis of axial velocity oscillations.

applying a Poisson type pressure correction equation using the continuity equation residue over each cell. After solving for the flow variables of velocity components and pressure, the temperature field is updated using the heat balance equation (4). The time marching procedure is continued until the steady state or a time-independent oscillatory solution is achieved. The convective terms are handled by QUICK scheme in the flow direction, while the diffusion terms are approximated by central difference over a nine point molecule. Although the numerical scheme provides spatially second order and temporally first order accurate solution, the flow and thermal oscillations have been captured well by using small non-dimensional time steps in the range of 10^{-4}–10^{-5} for the simulation. In each time step, the nodal pressure and velocity values are converged to a tolerance level of 10^{-6}. Since jet oscillations are expected to originate in the shear layer regions, a non-uniform mesh with fine spacing close to the nozzle exit in the axial direction and around the periphery of the jet in the lateral direction, has been employed. A detailed parametric study has been carried out by varying the non-dimensional parameters of Reynolds number Re ($=u_j d_j/v$) and Grashof number Gr ($=g\beta(T_j - T_0)d_j^3/v^2$) independently. The flow and temperature oscillations have been monitored at different dimensionless axial and lateral locations. The results predicted by the numerical simulation are presented in the following sections.

3. Results and discussion

3.1. Grid independence study and validation

In order to assess the grid independence of numerical results, a grid sensitivity study has been undertaken using the grids of 151×81, 201×101 and 151×121 nodes for the isothermal flow at $Re = 42$. For the different grids considered, the first and second indices correspond to the number of points in the axial and transverse directions respectively. As seen from Fig. 3, the variation in the mean velocity profile with grid refinement is minor and hence, a standard grid of 201×101 nodes has been used in all subsequent simulations. In few cases where larger domain length in the axial direction was required, even larger number of grid points than the standard case have been employed.

The predicted dimensionless velocity profiles at different axial locations have been compared for a jet Reynolds number of 42 with the experimental results of Sato and Sakao [3] in Fig. 4. A slit with aspect ratio of 50 was employed in the experiment, while theoretically the flow simulation has been treated as two-dimensional. The predicted mean velocity distributions at different stations ($x/d_j = 5$, 25, and 50) are compared with the corresponding experimental data. The agreement between the experimental and numerical results is excellent, at all the axial locations considered.

The u velocity variations with respect to time have been analyzed for different Reynolds numbers to evaluate the frequency of flow oscillations. The Strouhal number (S) has been calculated for different slit Reynolds numbers using the definition

$$S = \frac{f d_j}{u_j}$$

where $f =$ frequency of oscillations, $d_j =$ jet width and $u_j =$ slit centerline velocity. The predicted Strouhal number values are compared with the experimental results of Sato and Sakao [3] in Fig. 5. In the experimental data, some scatter was observed in the measured frequency values depending on the location where mea-

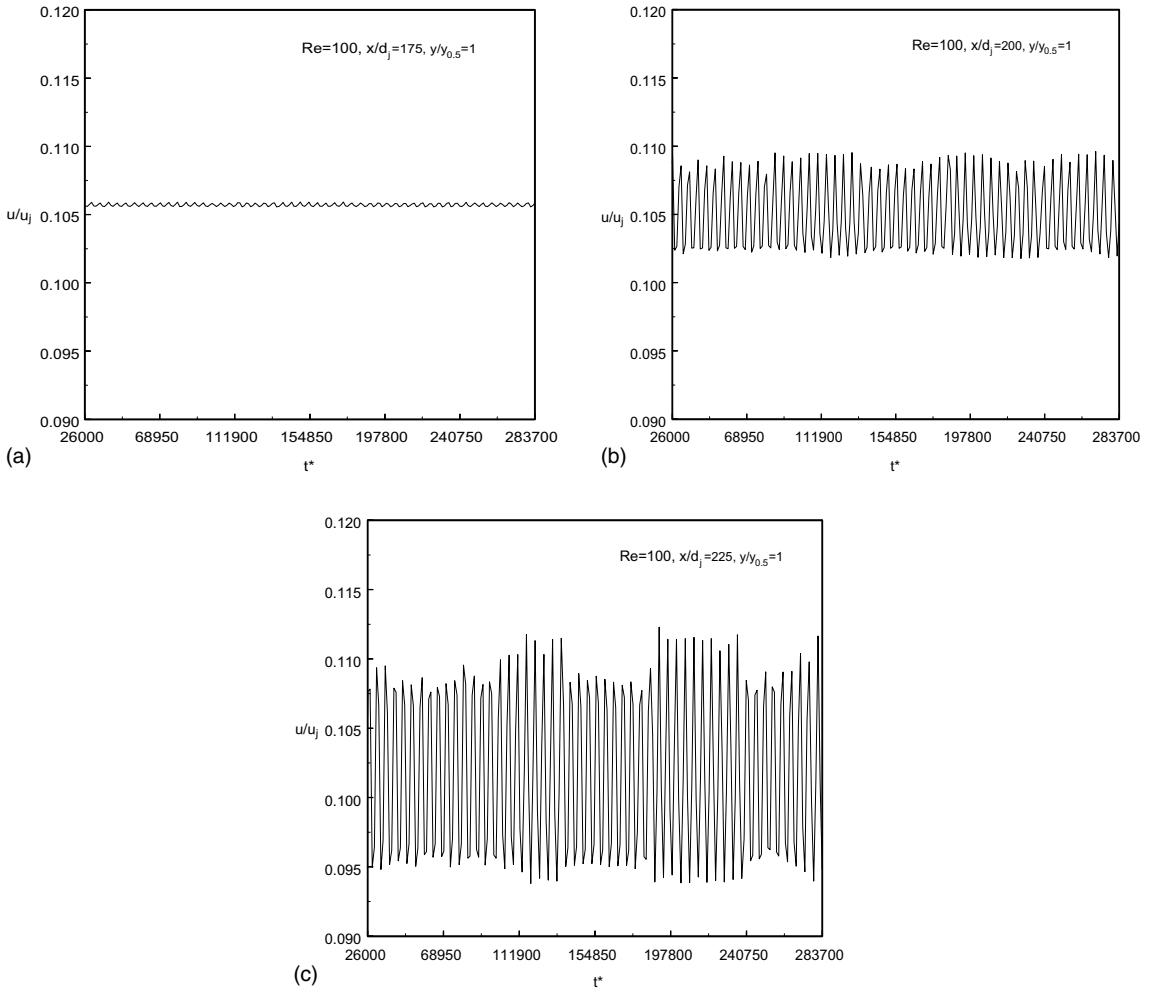

Fig. 9. Axial velocity oscillations: (a) $[x/d_j = 175]$, (b) $[x/d_j = 200]$ and (c) $[x/d_j = 225]$.

surements were made. It is evident that the predicted data for $x/d_j = 90$ and $y/d_j = 5$ lie in the range of measured Strouhal number values.

3.2. Flow oscillations in isothermal jet

The characteristics of velocity oscillations were first simulated for isothermal jets at different Reynolds numbers. The Reynolds number variation has been achieved by varying the average velocity at nozzle exit in the range of 2.98–7.45 m/s, with the jet width kept constant at 0.2 mm for air flow.

The mean axial velocity distribution along the centerline of a free jet at the Reynolds number of 40 is shown in Fig. 6(a). The centerline velocity decreases in inverse proportion to $x^{1/2}$, in accordance with the fully developed similarity profile for a plane jet [18]. The half width $y_{0.5}$ of the jet (the location where the axial velocity becomes the 50% of the centerline value) has been plotted as a function of dimensionless axial distance for $Re = 40$ and 100, in Fig. 6(b). After a rapid growth near the nozzle exit, the jet half-width variation becomes approximately linear for large axial distances. As mentioned earlier, the increase in jet width and decrease in centerline velocity are such that Reynolds number is the order of 100 everywhere.

Velocity fluctuations for the Reynolds number of 40 are shown in Fig. 7(a)–(c) at different spatial locations. The y location has been selected such that it falls in the middle of the shear layer where flow oscillations are predominant; in fact, the scaled distance $y/y_{0.5}$ has been kept same (equal to 1.0) at different axial locations. It is observed from the figures that the amplitude of velocity oscillations increases with axial distance, while the mean

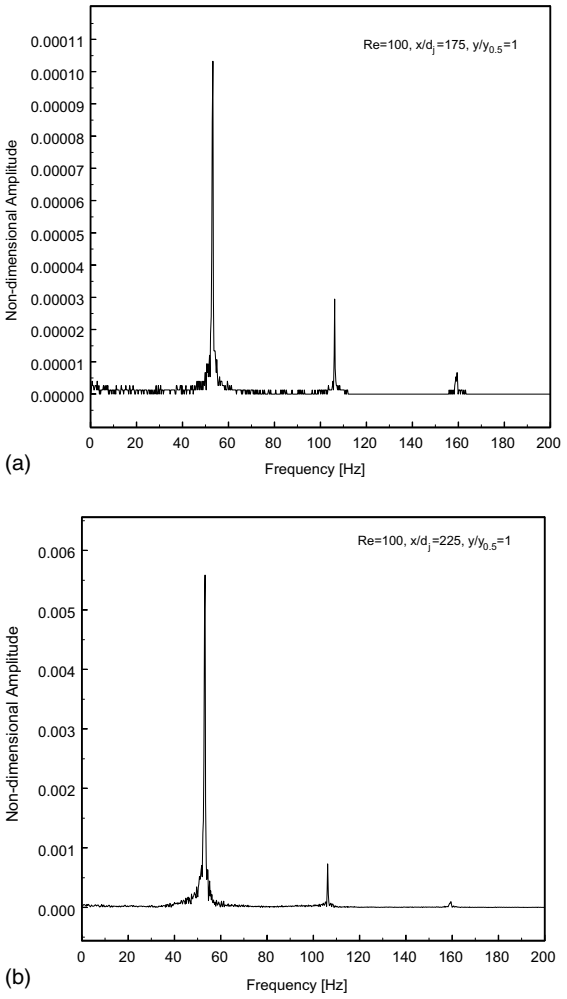

Fig. 10. FFT analysis of axial velocity oscillations: (a) $[x/d_j = 175]$ and (b) $[x/d_j = 225]$.

velocity value is more or less same. The trends indicate that the oscillations caused by convective instabilities in the shear layer amplify in the x direction, for the range of axial distances considered here.

Fast Fourier transform of the axial velocity oscillations for the above case has been carried out and the corresponding frequency spectra are shown in the Fig. 8(a) and (b). The FFT shows that the dominant frequency is 37.5 Hz for the case considered; however, higher harmonics are also present implying that the flow oscillations are not strictly sinusoidal, although they are periodic. The amplitude for each frequency component increases with axial distance, as evident from a close examination of Fig. 8(a) and (b).

Velocity oscillations have also been plotted for the Reynolds number of 100, at different locations (Fig. 9(a)–(c)). The corresponding FFT's are shown in Fig. 10(a) and (b). It is seen from these figures that the flow oscillations become non-periodic and correspond to higher frequencies (dominant frequency around 55 Hz) at $Re = 100$. The axial locations where oscillations commence are shifted away from the nozzle exit, implying that the shear layer growth is slower at a higher Reynolds number value. The same trend is evident in Fig. 6(b) also. An increase in amplitude of oscillations with axial distance is observed for $Re = 100$, similar to the case of $Re = 40$.

3.3. Flow and thermal oscillations in non-isothermal jets

3.3.1. General features

In order to estimate the relative magnitudes of forced and natural convective effects, simulations have been carried out for different Reynolds and Grashof number combinations for non-isothermal horizontal jets. In other words, the Richardson number ($Ri = Gr/Re^2$) has been varied in the range of 0.01–2.82 for these simulations (by varying the jet fluid temperature in the range of 300–360 K and the jet width in the range 0.2–8 mm), and the flow as well as thermal oscillations are analyzed.

For the forced convection dominated case of $Re = 40$ and $Gr = 564$, the dimensionless temperature oscillations are shown in Fig. 11(a)–(c). The velocity oscillations were somewhat similar to the isothermal case and hence they have not been shown here. It is evident that oscillations are periodic with the dominant frequency almost coinciding with the isothermal case discussed earlier (see Figs. 8 and 12). Moreover, increase in the amplitude of oscillations with axial distance is observed in the temperature fluctuations also. It is interesting to note that the inception of thermal oscillations has not occurred for $Re = 40$ at $x/d_j = 60$ in the mixed convection case (Fig. 11(a)), while velocity oscillations are indeed observed for the similar forced convection case in Fig. 7(a); this minor difference can be attributed to the fact that thermal diffusivity is larger than momentum diffusivity (i.e. $Pr < 1$) for air. In fact, the oscillations are caused by convection instabilities in the jet shear layer. A larger diffusivity value provides greater damping and hence thermal oscillations are damped more than velocity oscillations for $Pr < 1$.

Fig. 13 shows the variation in the dominant frequency of oscillations for velocity as well as temperature with Reynolds number. Although the initial variation of frequency with Reynolds number is non-linear, for $Re > 100$, a linear trend is observed. This implies that for a fixed jet width, both the frequency and Reynolds number vary linearly with the jet inlet velocity. Fig. 14(a) shows the spatial dependence of frequency in both x and y directions. While no changes are observed in the lateral (y) direction, higher

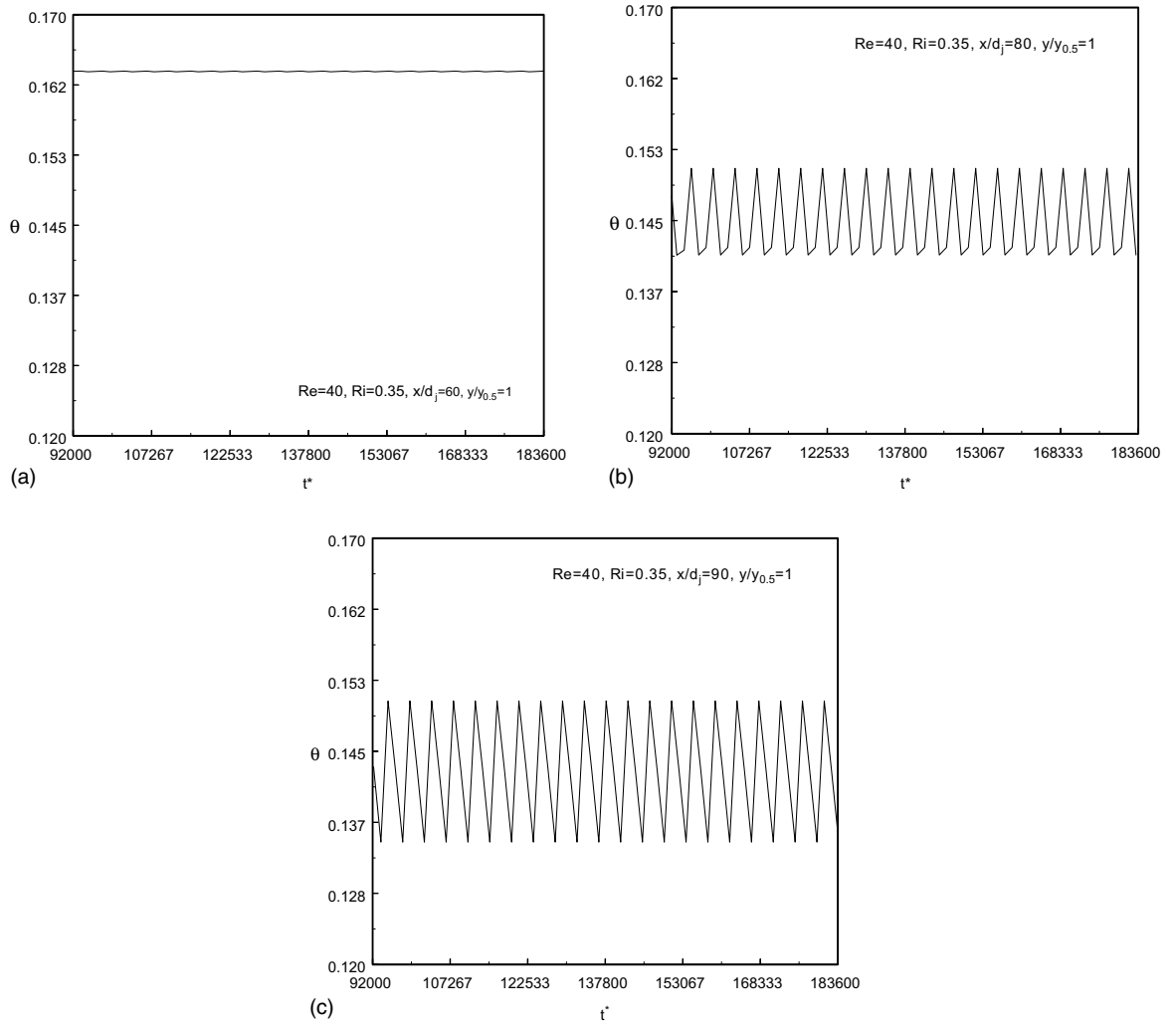

Fig. 11. Temperature oscillations in a buoyant horizontal jet: (a) $[x/d_j = 60]$, (b) $[x/d_j = 80]$ and (c) $[x/d_j = 90]$.

harmonics are seen at shorter axial distances. The variation in spectral distribution in the x-direction agrees with the well known trend that higher frequency components penetrate less than lower frequency components. Fig. 14(b) depicts the spatial variation in the amplitude of fluctuations. The peak value of amplitude occurs in the mid-portion of the shear layer in the y direction. In the axial direction, amplitude increases with distance initially but it later decreases after attaining a peak value (Fig. 15(a) and (b)). It is clear that the convective instability grows with distance from the nozzle as the shear layer develops, but it eventually decays due to entrainment and mixing of the jet fluid with the ambient fluid. For air having Prandtl number equal to 0.71, thermal fluctuations have slightly larger amplitudes than velocity fluctuations, although they originate at a larger axial distance.

The temperature fluctuations for a natural convection dominated situation are shown in Fig. 16(a) and (b). The remarkable feature here is that the oscillations correspond to low frequency fluctuations in the range of around 0.1 Hz. Also, the oscillations are not perfectly periodic and they contain spectral components over a range of frequencies. Such observations are in conformity with thermal striping phenomena reported in literature [1]. In Figs. 17 and 18, the spatial variations in the amplitudes of flow and thermal oscillations are depicted for a buoyancy dominated, horizontal jet configuration. It is to be kept in mind that although the jet starts as a symmetric forced convective flow, the buoyancy effects give rise to asymmetric flow development at larger x/d_j values (Fig. 19). These changes in flow structure influence the growth of fluctuation amplitude also. It is interesting to note that the flow and thermal

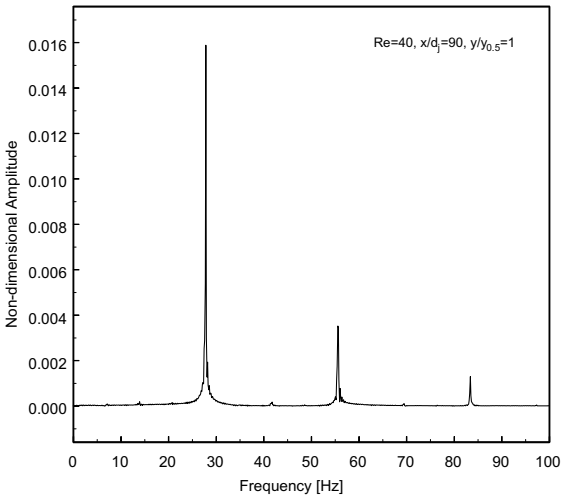

Fig. 12. FFT analysis for temperature oscillations $[x/d_j = 90]$.

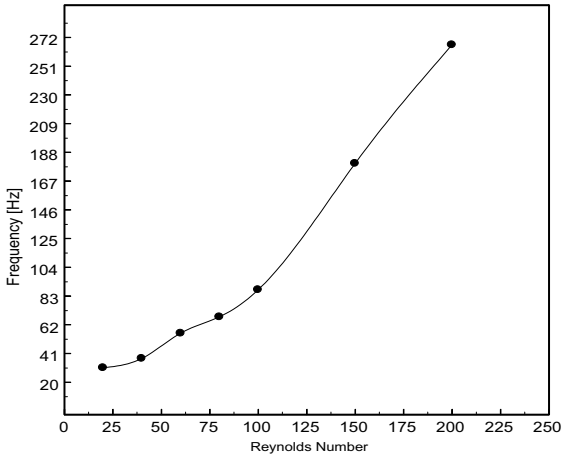

Fig. 13. Frequency variation of velocity and temperature fluctuations with *Re* $[x/d_j = 90,\ y/d_j = 5]$.

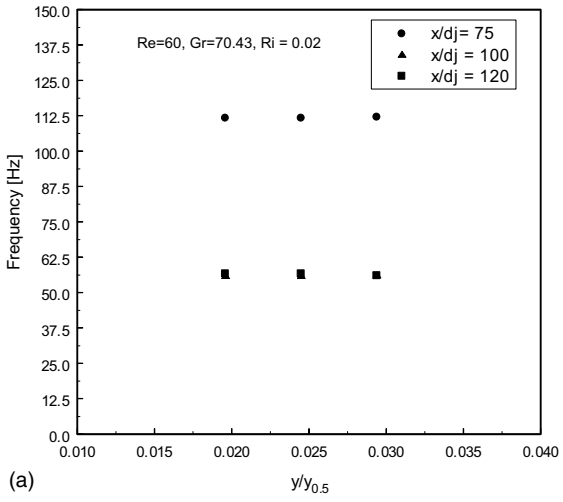

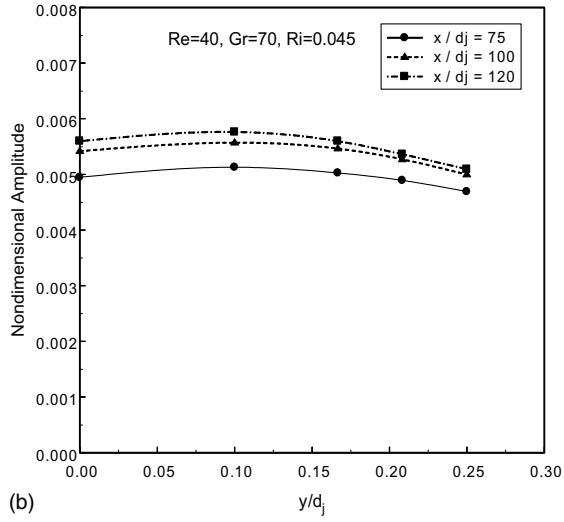

Fig. 14. (a) Spatial variation in frequency of velocity and temperature oscillations and (b) spatial variation in amplitude of velocity oscillations.

oscillations are out of phase spatially (Figs. 17 and 18), in this situation.

3.3.2. Orientation effects

The effects of jet orientation on fluctuations have been highlighted by considering three configurations, namely, horizontal jet, vertical upward jet and vertical downward jet. The FFT spectra for the velocity and temperature fluctuations at fixed values of *Re*, *Gr*, x/d_j and y/d_j are compared in Figs. 20 and 21, for different orientations of the jets. It is evident that the oscillations correspond to a band of frequencies. The spectrum is somewhat affected by the jet orientation, although the range of frequencies is more or less the same. The reason for these changes is seen in the Tables 1 and 2. It is evident that the jet development is different for different orientations. Hence, the difference in the variation of Strouhal number (based on dominant frequency) with axial distance differs for different jet orientations. In both Figs. 20 and 21, it is seen that the maximum amplitude occurs for the vertically upward jet; this can be easily explained by the fact that both forced and natural convective flow effects aid each other in this case.

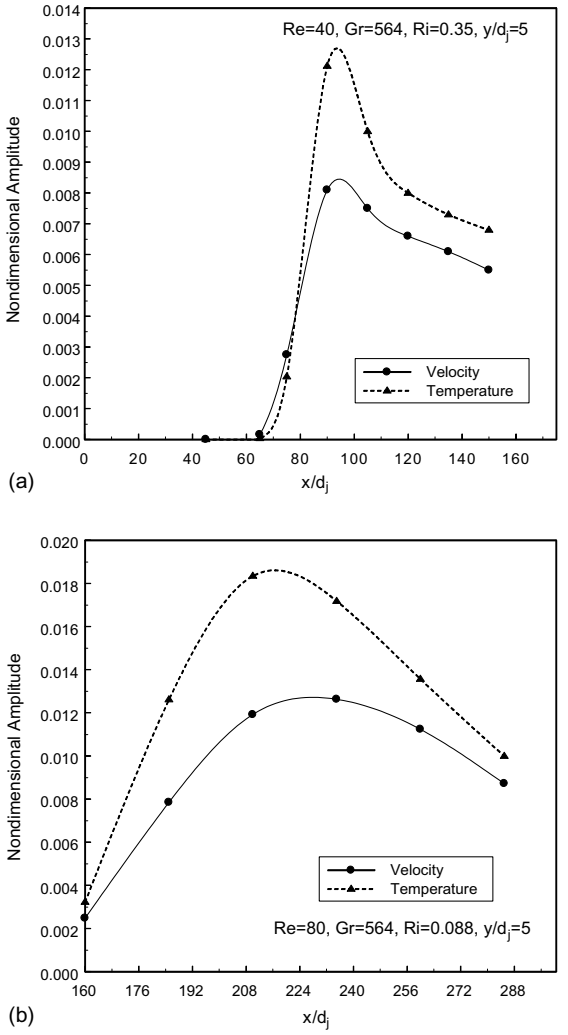

Fig. 15. (a) Variation in amplitude of velocity oscillations in axial direction [$Re = 40$] and (b) variation in amplitude of oscillations in axial direction [$Re = 80$].

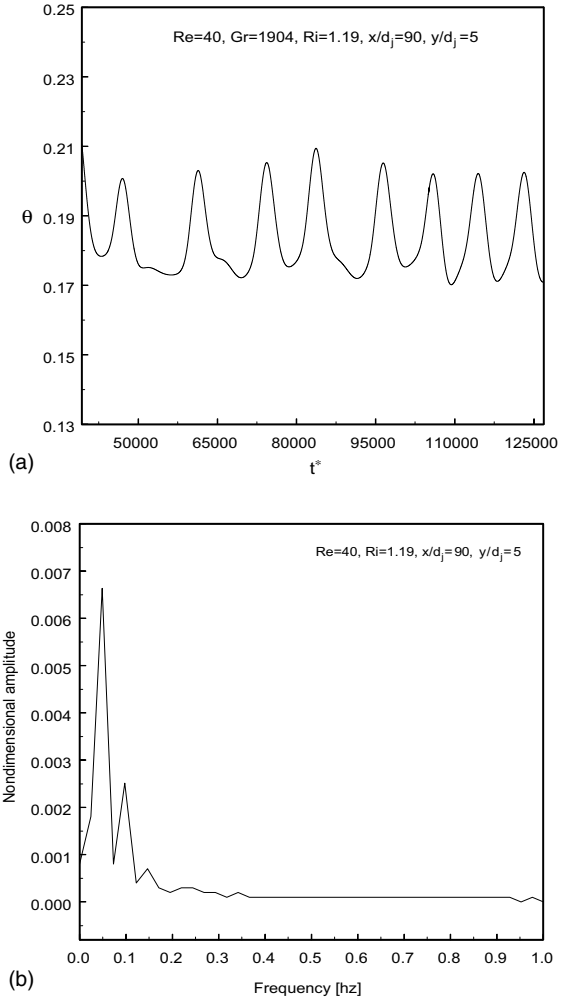

Fig. 16. (a) Variation in temperature oscillations [$Ri = 1.19$] and (b) FFT for temperature oscillations [$Ri = 1.19$].

4. Conclusions

The flow and thermal oscillations arising due to convective instability in a laminar two-dimensional jet have been analyzed in forced as well as mixed convection regimes, for different jet orientations. For isothermal jets, the frequency of velocity oscillations increases with Reynolds number and the axial location for the onset of oscillations also increases. At low Reynolds numbers, periodic oscillations are observed and at high Reynolds numbers, the oscillations contain a range of frequencies. In general, the spectra contain high and low frequency components in the near field, and only low frequency components in the far field. The amplitude of oscillations increases with axial distance initially, attains a peak value and then decays with distance. In the transverse direction, peak amplitude value occurs somewhere in the middle of the shear layer. When natural convective effects become predominant, the oscillations contain a broad band of very low frequency components and oscillations are not periodic even at low Reynolds numbers. The jet orientation does influence the flow development in the mixed convective regime. Also the spatial growth of thermal and velocity oscillations depends on whether the jet is vertically up, vertically down or horizontal, although the frequency range for the oscillations is more or less the same. The numerical predictions of the present study are in reasonable quantitative as well as qualitative agreement with available experimental data on related problems.

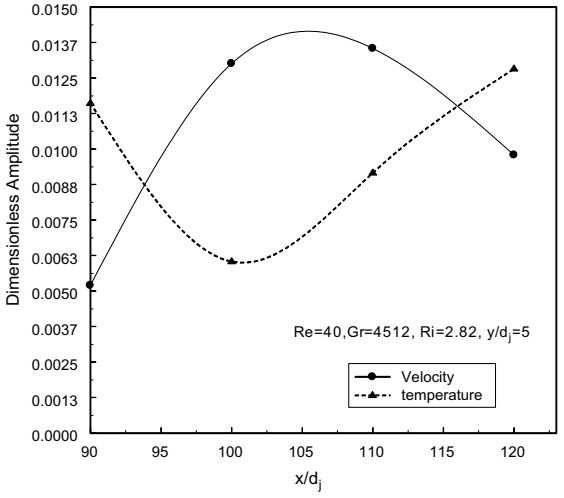

Fig. 17. Axial variations in amplitude of velocity/temperature oscillations for horizontal jet.

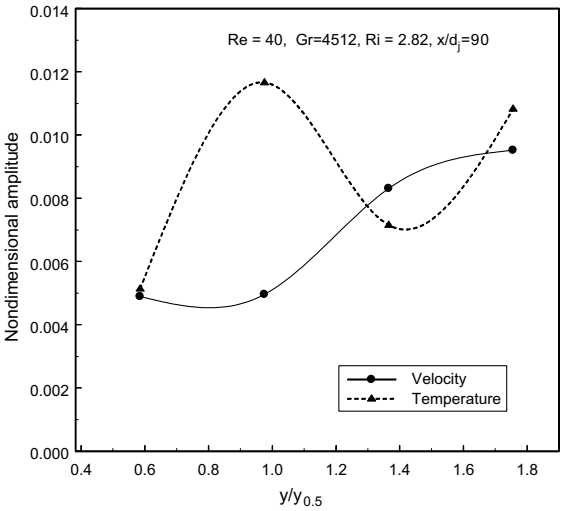

Fig. 18. Variations in amplitude of velocity/temperature oscillations in transverse direction.

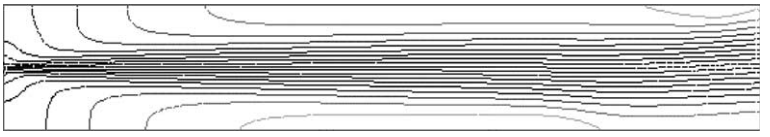

Fig. 19. Instantaneous streamlines for $Ri = 1.89$.

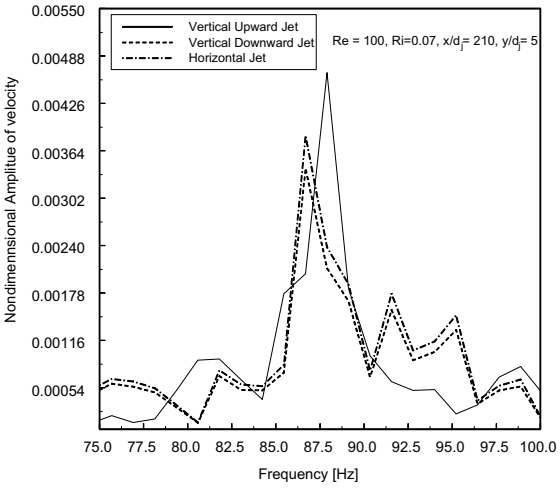

Fig. 20. FFT analysis of velocity oscillations for different orientation of jets.

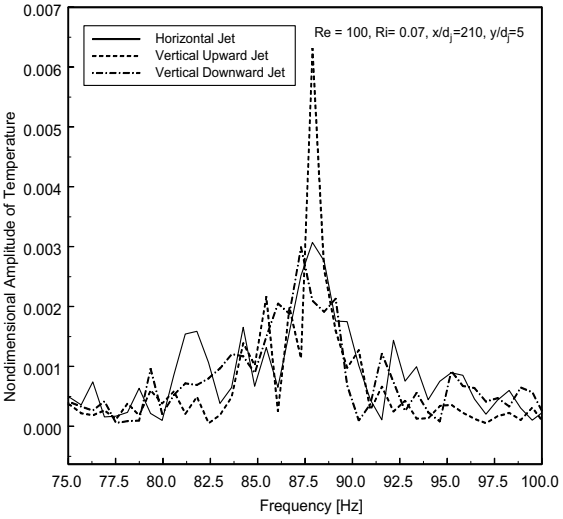

Fig. 21. FFT analysis of temperature oscillations for different orientation of jets.

Table 1
Variation of Strouhal number with dimensionless x distance $[x/d_j]$ for low Richardson number $[Ri = 0.3523]$

x/d_j	Strouhal number $[S]$		
	Horizontal jet	Vertical upward jet	Vertical downward jet
90	0.00353	0.00244	0.00352
100	0.002325	0.002325	0.002234
110	0.002325	0.002325	0.002325
120	0.00229	0.00229	0.00227

Table 2
Variation of Strouhal number with dimensionless x distance $[x/d_j]$ for high Richardson number $[Ri = 2.82]$

x/d_j	Strouhal number $[S]$		
	Horizontal jet	Vertical upward jet	Vertical downward jet
90	0.003860	0.0024890	0.002290
100	0.002789	0.0025032	0.002682
110	0.002682	0.0039378	0.002500
120	0.002040	0.0026820	0.001909

References

[1] M. Wakamatsu, H. Nei, K. Hashiguchi, Attenuation of temperature fluctuations in thermal striping, J. Nucl. Sci. Technol. 32 (8) (1995) 752–762.

[2] H. Sato, The stability and transition of a two dimensional jet, J. Fluid Mech. 7 (1960) 53–80.

[3] A. Sato, F. Sakao, An experimental investigation of the instability of a two dimensional jet at low Reynolds number, J. Fluid Mech. 20 (Part 2) (1964) 337–352.

[4] F. Durst, A. Melling, J.H. Whitelaw, Low Reynolds number flow over a plane symmetric sudden expansion, J. Fluid Mech. 64 (1974) 111–128.

[5] R.M. Fearn, T. Mullin, K.A. Cliffe, Nonlinear flow phenomena in a symmetric sudden expansion, J. Fluid Mech. 211 (1990) 595–608.

[6] G.K. Batchelor, A.E. Gill, Analysis of the stability of axi-symmetric jets, J. Fluid Mech. 14 (1962) 529–551.

[7] J. Cohen, I. Wygnanski, The evolution of instabilities in the axi-symmetric jet, Part 1. The linear growth of disturbances near the nozzle, J. Fluid Mech. 176 (1987) 191–219.

[8] A.S.R. Sarma, T. Sundararajan, V. Ramjee, Numerical simulation of confined laminar jet flows, Int. J. Numer. Meth. Fluids 33 (2000) 609–626.

[9] E.J. Gutmark, F.F. Grinstein, Flow control with non-circular jets, Ann. Rev. Fluid Mech. 31 (1999) 239–272.

[10] A.K.M.F. Hussian, H.S. Hussian, Elliptic jets, Part 1. Characteristics of excited and unexcited jets, J. Fluid Mech. 208 (1989) 257–320.

[11] S. Koshigoe, E. Gutmark, K.C. Schadow, Initial development of noncircular jets leading to axis switching, AIAA J. 27 (1989) 411–419.

[12] W.R. Quinn, Streamwise evolution of a square jet cross section, AIAA J. 30 (12) (1992) 2852–2857.

[13] K. Srinivasan, E. Rathakrishnan, Studies on polygonal slot jets, AIAA J. 38 (10) (2000) 1985–1987.

[14] P.A. Monkewitz, P.A. Sohn, Absolute instability in hot jets, AIAA J. 26 (1988) 911–916.

[15] J. Peterson, Y. Bayazitoglu, Measurements of velocity and turbulence in vertical axi-symmetric isothermal and buoyant jets, ASME J. Heat Transfer 114 (1) (1992) 135–142.

[16] V.S. Patankar, Numerical Heat Transfer and Fluid Flow, Hemisphere Publishing Corporation, Taylor & Francis, 1980.

[17] S. Suyambazhahan, Numerical and experimental study of jet oscillations, Ph.D. thesis, Department of Mechanical Engineering, Indian Institute of Technology Madras, June 2003.

[18] H. Schlichting, Boundary Layer Theory, seventh ed., McGraw-Hill, New York, 1979.